JOURNAL OF MATERIALS RESEARCH AND TECHNOLOGY 2023;25:5751–5766

Available online at www.sciencedirect.com

jmr&t Journal of Materials Research and Technology

journal homepage: www.elsevier.com/locate/jmrt

Superhydrophobic zinc oxide/epoxy coating prepared by a one-step approach for corrosion protection of carbon steel

Suk Wy Yap [a], *Norhasnidawani Johari* [a,*], *Saiful Amri Mazlan* [a], *Syarifah Nur Aqida Syed Ahmad* [b,c,**], *Rizal Arifin* [d], *Noor Azlina Hassan* [e], *Mohd Aidy Faizal Johari* [a]

[a] *Engineering Materials and Structures (eMast) IKohza, Malaysia-Japan International Institute of Technology (MJIIT), Universiti Teknologi Malaysia, Jalan Sultan Yahya Petra, 54100, Kuala Lumpur, Malaysia*

[b] *Automotive Engineering Centre, Universiti Malaysia Pahang, 26600, Pekan, Pahang, Malaysia*

[c] *Faculty of Mechanical and Automotive Engineering Technology, Universiti Malaysia Pahang, 26600, Pekan, Pahang, Malaysia*

[d] *Department of Mechanical Engineering, Universitas Muhammadiyah Ponorogo, Jl. Budi Utomo No. 10 Ponorogo, 63471, Indonesia*

[e] *Department of Manufacturing and Materials Engineering, Faculty of Engineering, International Islamic University Malaysia (IIUM), Jalan Gombak, 53100, Kuala Lumpur, Malaysia*

ARTICLE INFO

Article history:
Received 5 April 2023
Accepted 2 July 2023
Available online 5 July 2023

Keywords:
Corrosion resistance
Superhydrophobic coating
Zinc oxide
Durability
Carbon steel

ABSTRACT

Corrosion in carbon steel (CS) has been an existing issue and it calls attention to the need for improved corrosion protection. At present, superhydrophobic (SHB) coating technology has piqued the interest of researchers as alternative means of mitigating metal corrosion. Herein, a one-step solution deposition process was used to prepare an SHB coating based on nano-zinc oxide/epoxy (ZnO/EP) on CS and its corrosion resistance performance was analyzed by the means of electrochemical analysis and compared with that of the blank CS metal and the regular coatings (plain EP and regular ZnO/EP). Results implied the as-prepared SHB coating shows remarkable improvement in corrosion protection for the substrate. Notably, it exhibited higher in both impedance modulus (|Z|) and coating resistance (R_c) results approaching 10^{10} Ωcm^2, than those of regular coatings by 3 orders of magnitude to that of plain EP (~10^7 Ω cm^2), and 1 order of magnitude to regular coating (~10^9 Ω cm^2), indicating its superior corrosion resistance performance. Besides that, the superior inhibitive effect of the SHB ZnO/EP (ZES) is also proven by the potentiodynamic polarization (PDP) results, in which the I_{corr} value is suppressed down to 2.08 × 10^{-11} A/cm^2, thereby achieving an excellent corrosion rate result of 3.38 × 10^{-11} mm/year. The exceptional barrier protection is ascribed to the presence of a stabilized air interlayer captured within the coating/electrolyte interface thus effectively blocking the penetration of electrolyte into the coating. This facile yet effective one-step

* Corresponding author.
** Corresponding author.
E-mail addresses: norhasnidawani@utm.my (N. Johari), aqida@ump.edu.my (S.N. Aqida Syed Ahmad).

https://doi.org/10.1016/j.jmrt.2023.07.013

processed SHB coating offers an effective route to improve the corrosion resistance performance of the CS metal and thereafter expand its potential applications.

1. Introduction

Carbon steel (CS) has been found as the most widely used engineering material across a broad range of applications, mainly in structural construction and machinery manufacturing owing to its superior mechanical robustness, machinability, and cost-effectiveness [1]. Among different CS grades, S50C medium CS which possesses high impact strengths and weldability is particularly used for machinery parts and structural components such as automotive clutch parts, crankshafts, and hydraulic clamps [2]. However, along with its high chemical activity in actual operating conditions, CS is highly corrosive when exposed to aggressive conditions such as chlorine, oxygen, and water [3]. Over decades, several strategies have been adopted to mitigate its corrosion issue including electrochemical protection, protective coatings, and corrosion inhibitors [4]. Protective coatings are highly preferred in many industries due to their superior physical strengths, processability, and economical advantages, among which epoxy resin (EP) is highly favoured [5]. EP resin, as a long-established organic polymer coating is widely used for corrosion protection in harsh marine environments, especially for ships and marine structures as it possesses advantages such as outstanding mechanical stability, adhesion to metal, processability, and cost-effectiveness [6]. Nevertheless, the hydrophilic nature of EP is a critical limitation affecting its long-term durability in humid conditions, due to the presence of micropores that can simply permit the diffusion of water making it more susceptible to corrosion [7,8].

In recent years, significant research efforts have been devoted to controlling water repellency with the introduction of superhydrophobic (SHB) properties to the coatings as its inherent passive barrier layer can offer excellent corrosion resistance to the CS metals [9]. In addition, SHB coatings can also deliver other properties including self-cleaning [10], self-repairing [11], anti-frost [10,12], and oil/water separation [13] to the CS metal. The prerequisites to constructing an SHB surface are high surface roughness at the micro/nanoscale and low surface energy [14]. The SHB surface can effectively resist corrosion by the virtue of the unique hierarchical rough structure of the surface that can provide a stable layer of retained air, serving as a barrier film that blocks the infiltration of corrosive ions across it [15]. Various techniques have been proposed to develop SHB coatings on different metals such as soft lithography [16], hydrothermal [17], solution intercalation [18,19], spin coating [20], sol-gel [21], anionic polymerization [22], and grafting [23]. Nevertheless, most approaches encountered drawbacks limiting their widespread for scalable applications: expensive and laborious processing, costly equipment or exotic chemicals required, and slower processing speed [20]. Hence, this reflects the demand for a cost- and time-effective strategy to fabricate SHB coating for corrosion protection. At present, the fabrication of SHB coating utilizing nanoparticles with specific properties to generate multiscale roughness and to enhance the performance of polymeric coatings has emerged as a competitive strategy owing to its many advantages not only in terms of cost, and scalability but effective tunability of the coating properties can be achieved with ease by varying the coating formulation [24].

ZnO nanoparticles with multifunctional properties are of great interest. As one of the inorganic metal oxides, ZnO portrays a wide range of interesting physicochemical properties: photoelectrical, piezoelectric, antimicrobial, anti-ultraviolet (UV), and thermal-conductivity properties [25–27]. Moreover, the additional virtue given by the utilization of nano-ZnO to develop hierarchical rough surface structure in superhydrophobic surface fabrication is that it is a bio-safe, non-toxic and, chemically stable, cost-effective option [28]. Since EP alone is insufficient to provide a substantial corrosion barrier to CS due to its hydrophilic nature, the addition of inorganic nanoparticles, namely ZnO does not only improve the hydrophobicity of the composite system, it produces a tortuous pathway for the diffusion of ion and delays the ion penetration, thus further improving the corrosion protection [9]. Zhou et al. [15] prepared an SHB coating on magnesium alloy based on cluster-like ZnO/EP with a series of steps: etching, and spraying of ZnO/EP, followed by modification using stearic acid (STA). Owing to the double protection formed due to the existence of retained air layer and the interdigitated micro-nano structures from the coating itself, the sample achieved a large capacitive arc with a considerable impedance value approaching ~10^5 Ωcm^2. Unfortunately, the STA that exists as the top layer can be easily removed or dissolute and causes a loss in Cassie's superhydrophobic properties, which will consequently lead to a decline in corrosion protection [29,30].

Another study by Li et al. [31] also reported an SHB coating based on modified TiO_2 compounded ZnO/EP on the iron sheet. They first prepared modified TiO_2 through a hydrothermal process and modified ZnO using a one-pot method, then only combine it with EP. STA was added at a later step as a surfactant with the purpose to reduce the surface energy of the EP cross-linked product. The Nyquist diagram of the sample showed a substantial result of 10^3 Ω/cm^2 accredited to the firm metal-polymer interface and low free volume in EP. They noticed the molecular wrapped around affects the particle by EP arises the challenge for the formation of single-layer SHB coating on the substrate. Wang et al. [32] also reported STA functionalized ZnO/EP/fluorinated ethylene propylene SHB coating on an aluminum plate. The process involved a few treatments including modification of ZnO with STA, the addition of NH_4HCO_3 as a pore-forming agent, spray coating, and heat treatment. In the observation, the sample exhibited a good impedance result of 10^7 Ω/cm^2, attributed to

the conditions of air pocket formation leading to contact inhibition with the contaminant. Nevertheless, they observed the coating lost corrosion resistance after the loss of air pockets as the water can enter through the weak interface of the coating. Although these methods are still indeed effective in the corrosion protection of metal, it is not focused on the CS. Being a preferred material for many applications, the corrosion protection of CS using a rapid, straightforward yet effective route is of practical importance for scalable production and wide applications.

Besides that, these employed methods were still far-fetched to be used for widespread applications due to the complications involved since separated treatment processes are necessary to develop the superhydrophobic structure. The disadvantages of these multiple-step strategies are such as slow process, high energy consumption due to long heating, reliance on heating equipment, high cost, and the usage of toxic chemicals including fluorine and acetone. In particular, Most literature found in these superhydrophobic coatings was reported on using the hydrophobic agent, STA priorly to reduce the surface energy of the individual component or incorporating it as the top layer in their procedures [30]. Yet, there is a lacking of the role of STA in these coating systems to modify the EP matrix, thus igniting the challenges in constructing desired surface texture as the EP can overlay the nanoparticles due to undesired particles/polymer interaction [33]. Although earlier literature demonstrated STA as a coupling agent in their EP-based nanocomposites [34–36]. These reports demonstrated an enhancement in interfacial adhesion within the particle/matrix and the components' compatibility, allowing the particle to be fixed in the multi-dimensional cured EP network. Nonetheless, there is yet a fabrication strategy on the superhydrophobic coating that has reported on combining STA directly into their coating for this purpose. Thence a wiser strategy to achieve a superhydrophobic surface is using a one-step process with the direct incorporation of STA to modify the composite mixture.

Herein, in this study, considering the importance of corrosion resistance for the CS surface, the corrosion performance of the SHB coating on the S50C CS metal based on ZnO/EP prepared using the one-step coating deposition process has been evaluated. Electrochemical measurements of the coating including electrochemical impedance spectroscopy (EIS) and polarization tests were conducted and compared with the blank CS substrate, as well as the plain EP and regular ZnO/EP coating on CS. Further investigation of the surface morphology and chemical composition of the samples, as well as the schematized illustrations demonstrating the efficacy of the SHB coating as a barrier against the corrosive medium to reach the CS surface.

2. Materials and methods

2.1. Materials

S50C graded medium CS with a chemical composition of 0.47 wt% C, 0.21 wt% Si, 0.58 wt%, Mn, 0.015 wt% P, 0.002 wt% S, and 0.300 wt% Cr and Fe as balance manufactured by Special Steel & Alliance Pte Ltd., Kuala Lumpur, Malaysia was used as the substrate. ZnO nanoparticles with an average diameter ranging <50 nm and STA of reagent grade were purchased from Sigma Aldrich, St Louis, MO, USA. Commercial EP resin of diglycidyl ether of bisphenol A (DGEBA) grade with resin: hardener ratio 2:1 was obtained from Sky Tech Malaysia Pte Ltd., Selangor, Malaysia. Absolute ethanol was purchased from Merck Millipore, Darmstadt, Germany. Deionized water (DI) purified in an ultrapure water system (Nanopores) was used in the experiment.

2.2. Samples fabrication

The CS metal pieces were cut into the size of $25 \times 25 \times 2$ mm^3 using a CUT20P wire-cutting EDM machine (Agie Charmilles, Losone, Switzerland). The workpieces were then polished by an ACC84DX Precision Grinding Machine Model (Okamoto, Gunma, Japan) to remove rust spots and to obtain uniform surface roughness of 1 ± 0.5 μm each. Subsequently, the abraded metal pieces were ultrasonically cleaned with acetone to remove debris from their surface and dried at room temperature. The preparation process of the SHB ZnO/EP sample (ZES) is referred to as the method reported in our previous work [37]. Firstly, 0.6 g of ZnO nanoparticles and 2.5% wt./vol. of STA were dispersed in 10 ml of absolute ethanol with constant agitation of 180 rpm at 55 °C for 5 min, followed by ultrasonication for 5 min at 500 W, 20 kHz. Subsequently, 0.15 g of EP resin and its hardener were added to the suspension and mechanically stirred for 10min. The resulting coating solution was inoculated to the CS piece and tilted until the whole surface was coated. It was then dried at ambient temperature for 24 h. In addition, the samples with plain EP and ZnO/EP (ZE) composite without the addition of STA coated on CS substrates were also prepared and served as reference samples.

2.3. Chemical characterization

The surface morphologies of the as-prepared specimens using JSM-7800F field emission scanning electron microscopy (FESEM) (Japan Electronics, Tokyo, Japan), with the measured current of 10 A and an accelerating voltage of 5 kV. Before the test, the specimens were sputtered with a Platinum/Palladium layer of 150 nm thickness to remove surface charging. The chemical microanalysis was conducted with energy-dispersive x-ray spectroscopy (EDS). The 3D laser scanning confocal microscopy (LSCM) was used to obtain the 3D topography and surface roughness of the samples using the LEXTOLS4100 laser confocal microscope (Olympus, Tokyo, Japan). The phase compositions and crystal structures were characterized using a Paralytical Empyrean X-ray Diffractometer (XRD) (Malvern PANalytical, Netherlands, Europe) with a Cu Kα radiation source ($\lambda = 0.15406$ nm) at a scanning rate of 5°/min, in the diffraction angle (2θ) range of 10°–90°.

2.4. Wettability

The water contact angle (WCA) was measured with 8 μL of deionized water droplets according to the sessile drop method. The measurement of angles was taken subsequently in the obtained images using Image J software (National

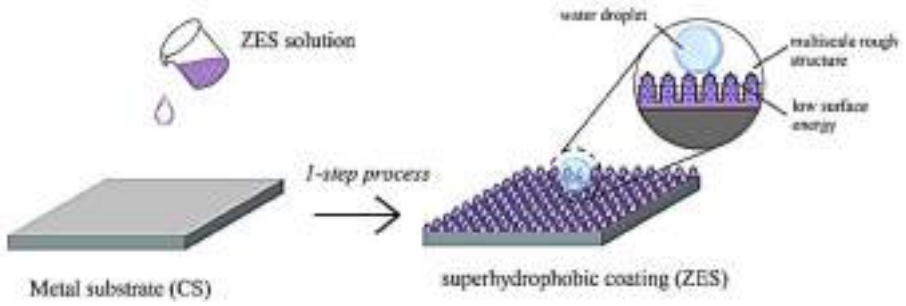

Fig. 1 – Schematic illustration of the SHB surface with robust hierarchical structures fabricated on CS substrate.

Institute of Health, USA) with a Low bond axisymmetric drop shape analysis (LB-ADSA) plugin. The average values of WCA were obtained by measuring three different spots on the sample surfaces.

2.5. *Electrochemical test*

The corrosion performance was characterized by electrochemical impedance spectroscopy (EIS) and potentiodynamic polarization (PDP) in a 3.5 wt % NaCl solution (pH≈6.0) at ambient temperature, using an Autolab PGSTAT100 Potentiostat (Metrohm, Riverview, FL, USA) with 1 μV resolution, and controlled by the NOVA 2.1.5 software (Metrohm, USA). Autolab applications including software FRA for EIS measurement and circuit fitting. Experimental parameters for PDP measurements were carried out according to ASTM G61 [38]. In a three-electrode system, the SHB surface-coated CS with an exposed area of 1 cm^2 was used as the working electrode (WE), platinum rod as the counter electrode (CE), and saturated calomel electrode (SCE) as the reference electrode (RE). Briefly, the samples were immersed at a stable open circuit potential (OCP) in the corrosive solution for 1 h before applying potential perturbation. The EIS was conducted at OCP in the frequency range of 10^{-2} Hz to 10^5 Hz with an amplitude of 10 mV. The PDP curve was recorded from −250 to 250 mV at a scan rate of 1 mV/s.

3. Results

3.1. *Microstructure morphology, chemical composition, and crystal structure*

Fig. 1 schematically illustrates the strategy for the fabrication of SHB ZnO/EP coating on the CS metal substrate effectively achieved by the one-step process proposed in this study. In this study, the one-step process for preparing the SHB coating (ZES) on the CS metal consists of four key components that are responsible for different roles in the system: STA as the surface modifier, ZnO nanoparticles to promote hierarchical-scale roughness, and EP as the adhesive to bond the coating to the substrate, and ethanol solvent to facilitate fast-drying and the formation of the dense network. Nonetheless, it is crucial to note that the hardest challenge to fabricating a one-layer SHB coating was avoiding the "wraparound effect" of the nanoparticles in the adhesive [31]. As generally in those approaches of using organic component such as EP to prepare SHB surface, it is important to regulate the ratio of both organic and inorganic material as the excessive organic component in the system will over envelope the inorganic elements, leading to insufficient roughness [33]. Therefore, adjusting the binder: particle ratio plays a key role in constructing sufficient hierarchical structures for the achievement of superhydrophobicity on the coating.

In consideration of achieving an adequate balance between the ease of processing, as well as the SHB and adhesion properties, the optimum ZnO: EP mass ratio of 4:1 was adopted [37]. Further investigation into coating adhesion also revealed that reducing EP resin content could compromise the coating adhesion and mechanical strength. This was evident with the coating with 5:1 ratio suffered damage and peeled off during instantaneous peeling experiment (Fig. 2a. These findings emphasize the importance of maintaining a balance composition to ensure good adhesion. Indeed, with an adequate amount of EP loading, the coating showed neither gap nor crack at the coating/substrate interface owing to the excellent adhesion of EP to the substrate, with a uniform thickness of approximately 18.77 μm ± 1.92, as shown in Fig. 2b.

On the other hand, another noteworthy aspect of this method is the role of STA in grafting onto the ZnO nanoparticles to form a hydrophobic monolayer. In this case, embedding ZnO nanoparticles into the EP matrix became inevitably challenging due to the improvement in hydrophobicity of the ZnO itself [39]. Therefore, this event is important to ensure less occurrence of the EP fully enveloping the nanoparticles, thus promoting the formation of multiscale structures. Fig. 1 schematically illustrates the strategy for the fabrication of SHB ZnO/EP coating on the CS metal substrate effectively achieved by the one-step process proposed in this study.

Fig. 3 reveals the surface and cross-sectional microscopic morphologies of the blank CS substrate and the coated surfaces (plain EP, ZE and the SHB ZES), taken at different magnifications by the FESEM analysis. As shown in Fig. 3a, the surface of blank CS presented a smooth surface with uniform polishing marks aligned parallel to the direction of one another after the machining process. However, for the plain EP-coated surface (Fig. 3b), some micro-voids and heterogeneous structures of <1 μm can be found in the cross-section. The presence of micro-voids could initiate larger size defects in the matrix, and impair the barrier performance of the

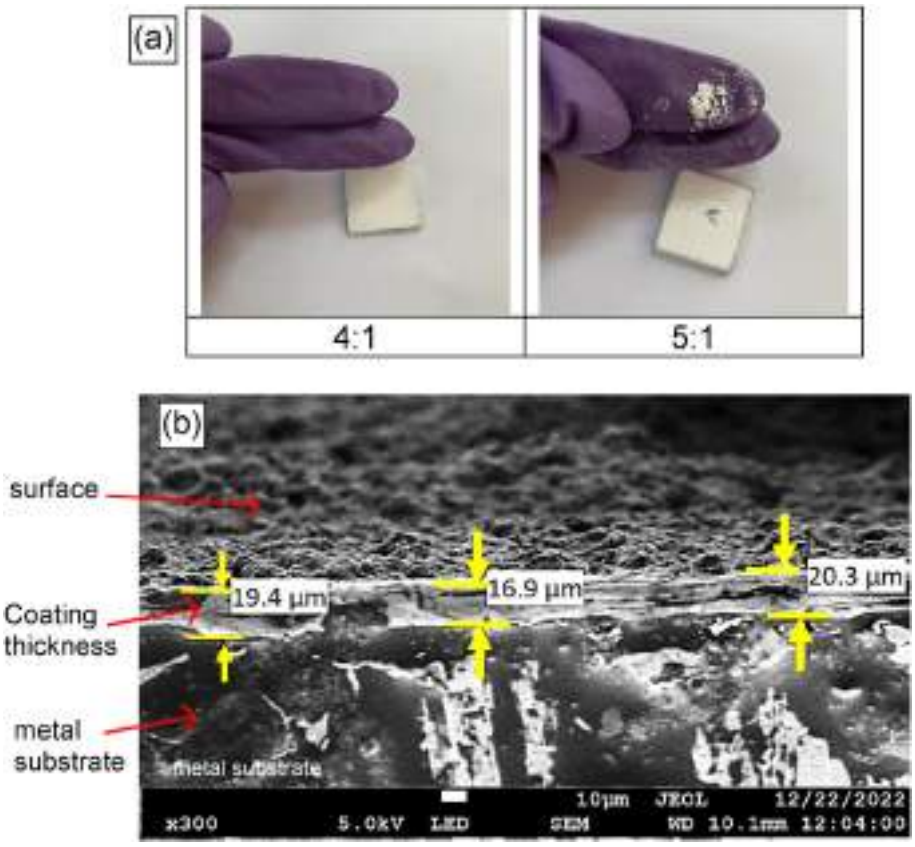

Fig. 2 – (a) Adhesion test on coating with 4:1 and 5:1 ZnO: EP mass ratio, and (b) SEM image portraying coating thickness.

coating [40]. Compared to pure EP film, the improvement in hydrophobicity of the ZnO/EP surface (Fig. 3c) is attributed to the aggregation of ZnO nanoparticles. After the addition of STA as the modifier, the surface roughness and morphology were greatly improved as shown in Fig. 3c–(f). This generated surface exhibits a high degree of hierarchical scale roughness. At the same time, low surface energy can entrap air within the rough asperities, preventing water infiltration. As a result, the coating exhibited superhydrophobicity [41]. This wettability behaviour conformed to the Cassie-Baxter model described in the literature, wherein water droplet to be suspended on the solid-air interface and trapped in the rough asperities.

The resulting SHB coating sample displayed randomly orientated irregular aggregates of ZnO nanocrystals (Fig. 3.3 (f), facilitating the formation of hierarchical micro/nano-roughness and it endows a large number of air cushions trapped within the binary scale structures [42,43]. Subsequently, this allows it to render exceptional permeation properties against the solution through the Cassie-Baxter contact. The presence of an air layer exists between the SHB surface and water, as demonstrated as gleaming mirror-like layer on account of reflection when immersed in water shown in Fig. 4. In contrast, the air layer was absent in the non-SHB coatings. This air layer plays an important role as a barrier to inhibit the corrosive agents to reach the underlying metal, thus improving corrosion protection [44]. In addition, compared to the EP sample, the number of microvoids sharply decreased after the incorporation of ZnO nanoparticles into the ZES sample, indicating the dispersed ZnO NP could effectively fill the micro-voids in the EP matrix. Fig. 3 (f) presents the close-up view of Fig. 3e with higher magnification, demonstrating that ZnO nanoparticles composed of different forms and sizes conglomerate together to construct a multi-scale rough surface, which is valuable to the improvement in hydrophobicity of the coating.

Surface roughness is of importance in the fabrication of the SHB surface. Fig. 5 presents the 3D topography images of the uncoated and coated samples as analyzed by the LSCM. The surface structure of the blank CS sample (Fig. 5a) was as smooth as that of the plain EP-coated sample (Fig. 5b). This result was in line with the microscopic images taken by FESEM (Fig. 3 a and b). As expected, the 3D images of the ZE and ZES samples (Fig. 5c and d) manifested binary scale roughness on the surfaces. Yet, the ZES sample particularly presented relatively richer surface topography than the ZE sample, indicating the contribution of STA modification on the ZnO/EP system in fostering substantial surface roughness to achieve SHB properties. The results of the 3D profile were in line with the presentation of microscopic images, denoting that the SHB properties of the coating may be closely related to the microscale roughness of the surface, and thus acknowledging the fabrication of SHB coating is possible to be accomplished by the one-step method in this study.

Generally, the parameters including arithmetic average roughness (R_a) and root-mean-square roughness (RMS, R_q) of the prepared samples were used to present the surface roughness. As shown in Fig. 6, both R_a and R_q indicated a minimal increase when the blank CS substrate was coated

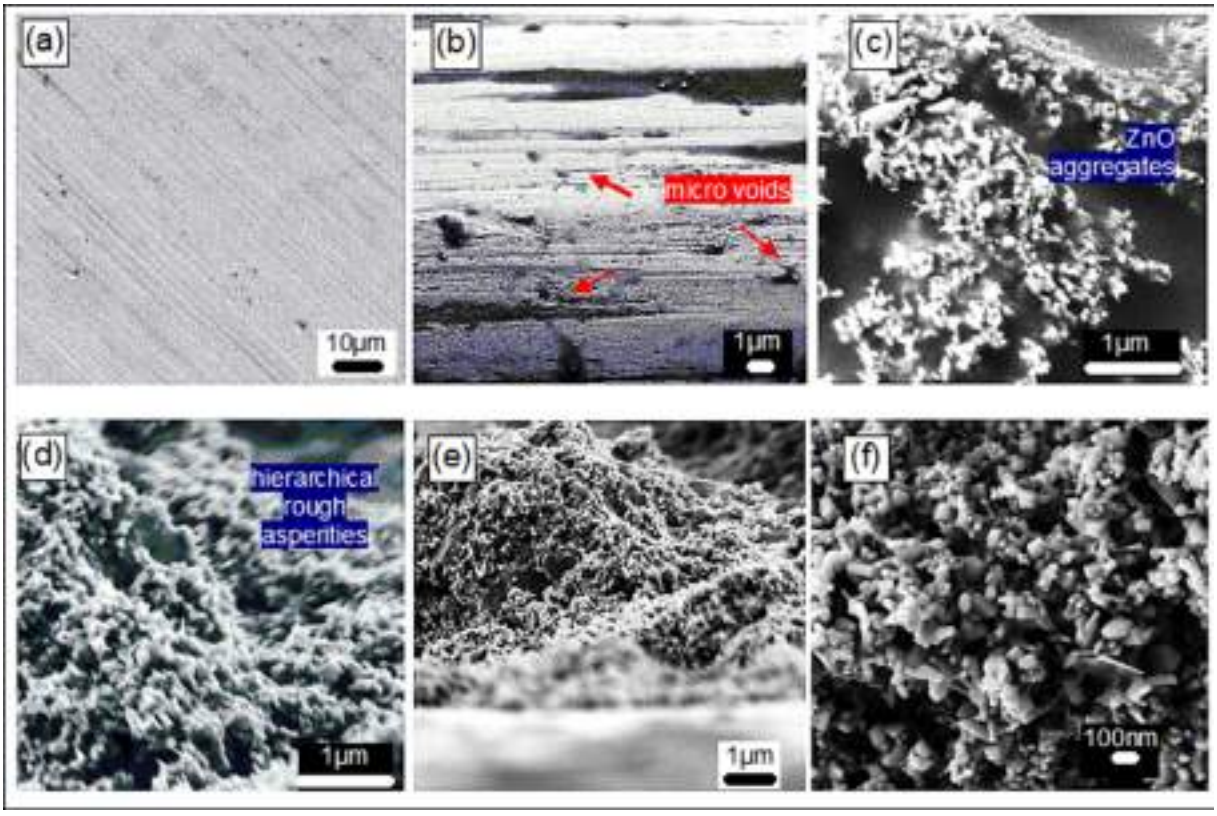

Fig. 3 – FESEM images of (a) blank CS substrate, and cross-sectional morphology of the (b) regular EP sample, (c) ZE sample at 20,000 magnification and the ZES sample at different magnifications: (d) 20,000×, (e) 8,000×, (f) 35,000×.

with plain EP with results from 0.215 ± 0.009 μm (R_a of CS) and 0.221 ± 0.013 μm (R_q of CS) to 0.8 ± 0.121 μm (R_a of EP) and 0.94 ± 0.141 μm (R_q of EP), respectively. These samples are yet too flat and smooth to construct a high-water-repellent surface. Conversely, the R_a and R_q results were higher for the ZE and ZES samples. Nonetheless, the R_a and R_q results of SHB ZES with values of 2.706 ± 0.30 μm and 3.569 ± 0.429 μm respectively were at least twice as higher as the regular coating (1.147 ± 0.150 μm and 1.424 ± 0.213 μm respectively). This indicates that surface roughness was enhanced after the introduction of STA, which promotes the formation of SHB structures.

The surface roughness is not the only factor determining the superhydrophobicity of the surface. Although a rough surface is by no means compulsory, this condition alone is insufficient to achieve superhydrophobicity for the surface. Achieving SHB surface emphasizes acquiring micro/nano-scale roughness that exhibits substantially low surface energy. In this study, both conditions of low surface energy and multiscale roughness can be attained just in one step. The ZnO/EP composite constitutes the robust rough structured surface, whereas the STA which has 18-carbon saturated long chains is introduced to promote low surface energy. To evaluate the modification by STA on the composite, FTIR,

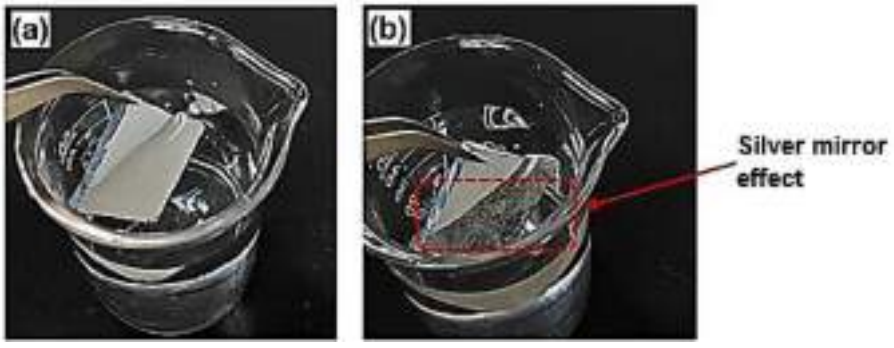

Fig. 4 – Observation comparison of (a) regular coating sample (ZE), and (b) SHB coating sample (ZES) when immersed in 3.5 wt% NaCl solution.

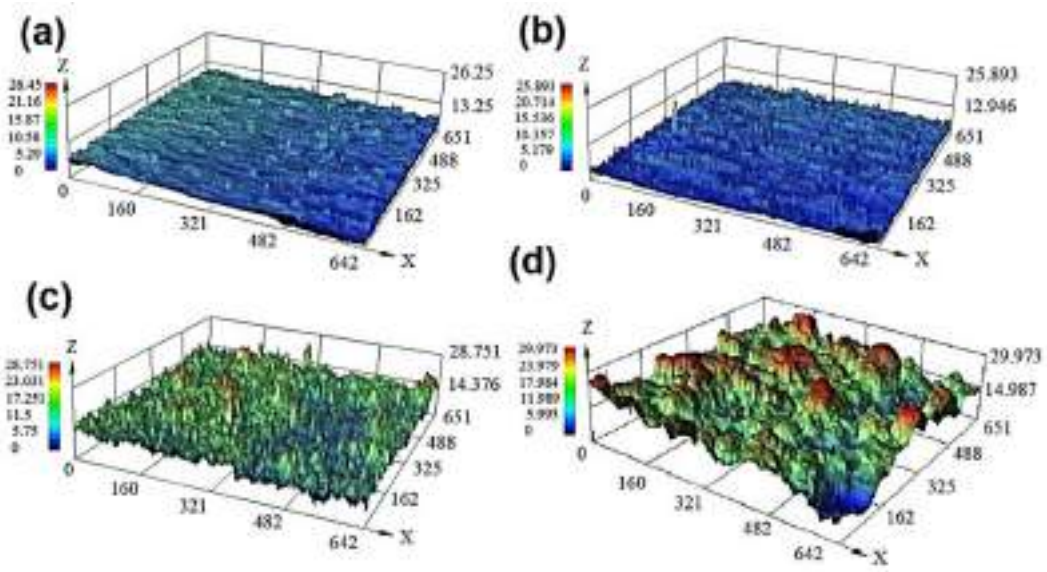

Fig. 5 – 3D LSCM images showing the surface microtopography of the (a) CS, (b) EP, (c) ZE, and (d) ZES samples, (μm).

EDS and XRD analyses were carried out in this study. Fig. 7 presents the EDS regional analysis and FTIR spectra of the regular coating (ZE), and the SHB coating (ZES), and comparisons are made with and without the presence of STA. As seen in Fig. 7, Zn, O, and C elements were detected. The detection of a relatively strong peak indexed to Zn in both spectra indicated that the ZnO nanoparticles were uniformly distributed throughout the coatings. Besides that, the number of C atoms increased from 9.96 to 16.38 wt% after the incorporation of STA into the composite, whereas the proportion of O and Zn decreases from 16.26 to 14.46 wt%, and from 73.78 to 69.16 wt% respectively. This suggested in the ZES sample, that part of the STA was bonded to the –OH group on the surface of the ZnO nanoparticles, and another part of STA was adhered to the surface by physical adsorption. Since a mole of STA holds 18 mol of C atoms, therefore, in the presence of STA addition, the mass content of the whole coating system of the sample increased along with the number of C atoms [15]. Besides that, the presence of the C-element adhered on the surface by physical adsorption convinced that the EP resin is partially exposed during the modification process, therefore in line with the proposed schematized mechanism of the as-prepared coating (Fig. 1). In addition to this, it can also be seen that the proportion of O-atom was lower than the Zn atoms indicating the presence of partial O atoms associated with the STA on the surface and its involvement in the modification reaction. Therefore, these results inferred that the role of STA is important in modifying the composite to develop the SHB surface, especially grafting onto the ZnO and the embedment of the nanoparticles in the matrix.

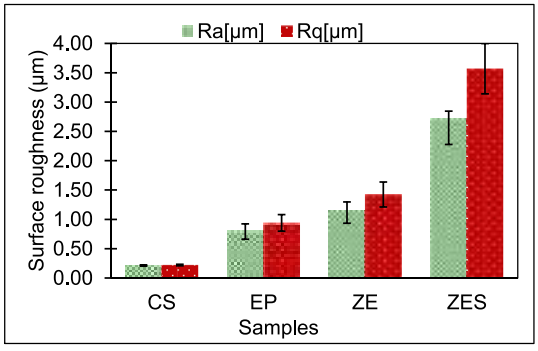

Fig. 6 – Surface roughness of blank metal and coated samples.

Additionally, FTIR analysis provides evidence of the absorption of SA on the surface of the ZES coating. We compared the FTIR spectra of the ZES with the ZE sample, as shown in Fig. 7c. Here the presence of a superhydrophobic layer composed of ZnO nanoparticles within the EP resin coating can be verified. Specifically, in the ZES spectra, we observed peaks at 2851 cm^{-1} and 2916 cm^{-1}, which corresponded to the symmetrical and asymmetrical C–H vibrations of the STA alkyl group [29,45]. This supports that the surface of ZnO nanoparticles is linked to the alkyl group of STA. indicating successful modification of both the ZnO nanoparticles and EP matrix. These results underscore the significant role of STA in modifying the composite to develop the superhydrophobic surface by grafting onto the ZnO and embedding them within the matrix. These findings align with the previous reports on FTIR observation of the SHB coatings using STA as a modifier [29,46].

To further evaluate the effect of hydrophobic modification on the ZES composite, the XRD analysis was carried out to investigate the composition of the coating. The diffraction pattern of the ZnO/EP composite with the STA modification (ZES sample) was shown in Fig. 8. The peaks in the spectrum match those of ZnO (JCPDS Card No. 36-1451, showing that the coating did not alter the crystalline structure of the ZnO (zincite) [47]. Besides that, the appearance of prominent peaks around 33.4° and 37.8° implies the presence of zinc stearate crystals (JCPDS Card No. 05-0079) in the ZES sample

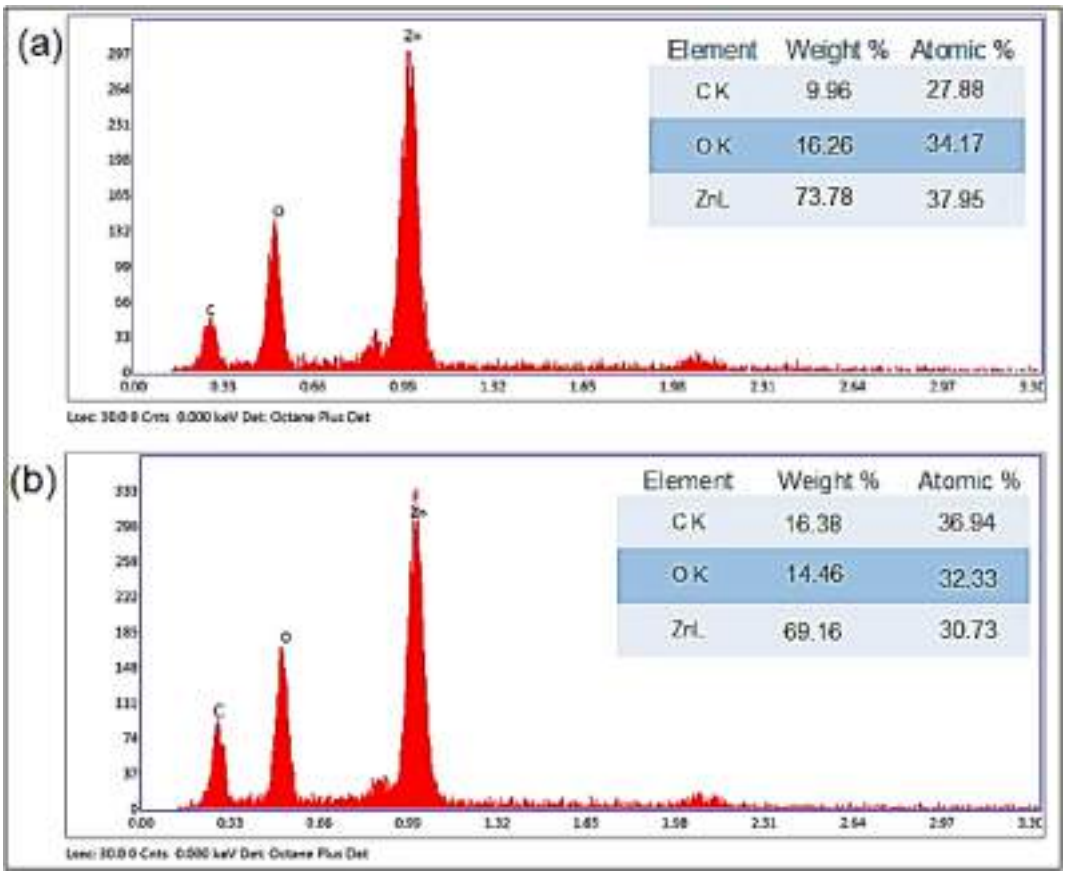

Fig. 7 – EDS (a) without and (b) with the presence of STA in the coatings.

[48–50]. As the ZnO nanoparticles carry a large number of –OH groups, the $-CH_3$ hydrophobic group from the SA tends to selectively graft onto the nano-ZnO to form a monolayer rather than interacting with the EP in the solution, successfully constructing an SHB coating on the surface of CS metal [51]. Thence it can be further deduced that this agrees well with the EDS results that the modification by STA on the ZnO/EP contributes to the successful fabrication of the SHB coating.

3.2. *Surface wettability of the coating*

It is known that the wettability of a solid surface is governed by both surface morphology and chemical composition [11]. For an SHB surface, the non-wettability behavior is associated with the presence of a substantial amount of air trapped inside the cavities of these roughened structures and extended at the air-liquid interface area that forms a barrier, subsequently hindering the penetration of water into the valleys

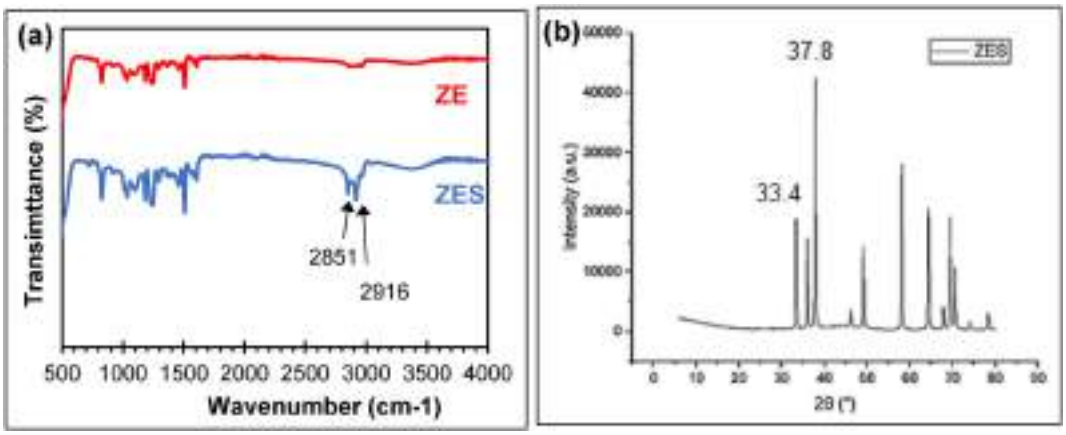

Fig. 8 – (a) FTIR spectra of both ZE and ZES samples, and (b) XRD pattern of the ZES sample.

and grooves of the surface. Fig. 9 shows the WCAs of different samples and the insets are the corresponding droplet images of each sample. As shown, the blank CS metal exhibits 71.60 ± 3.3° indicating the hydrophilicity of the original surface. The extremely easy-to-wet nature of the CS allows the water or ions to simply reach the surface, therefore susceptible to corrosion in the presence of water. Meanwhile, the WCA of the EP sample increased to ~81.28 ± 1.7°, which however still exhibits hydrophilic behavior, due to the intrinsic nature of EP containing large amounts of hydroxyl groups that are very reactive to water. However, when ZnO nanoparticles are introduced into EP coatings, the WCA of the ZE coating grows to 129.7 ± 1.3°, showing improvement in hydrophobicity attributed to the increased surface roughness. The result was in line with the LSCM analysis. This convinced the reality that attaining surface roughness alone is not enough to achieve superhydrophobicity for the surface as achieving SHB surface also requires low surface energy. Nonetheless, after incorporating STA into the ZnO/EP the WCA of the ZES sample increased to 165.13 ± 1.5° indicating superhydrophobicity of the coating. This is attributed to the reduced surface energy of the rough structure. Therefore, this proves that the SHB surface is the result of a synergistic effect between hierarchical multiscale rough structures and the low surface energy material [52]. Moreover, the result of the ZES was in line with the WCA result when coated on the glass substrate prepared in our previous work, which was 160.24° [37]. The ZES sample coated on CS in this study exhibited a slightly higher WCA result than that coated on glass suggesting the relatively better adhesion of the EP on the CS substrate. The outstanding metal/EP structural adhesion system on account of the extremely high surface energy of the metal surface that eventually leads to improved interfacial energy is thus known to contribute to the protection of metal including CS against different damaging environments [53]. Nevertheless, the WCA results of both samples were maintained at >150°, which is the SHB range, indicating the excellent versatility and stability of the as-fabricated SHB coating to be prepared on different substrates. Based on the excellent surface non-wettability results, the as-prepared SHB coating allows the CS to contact with water in Cassie-Baxter's mode, thus beneficial in obstructing the permeation of water into the coating and preventing the occurrence of corrosion.

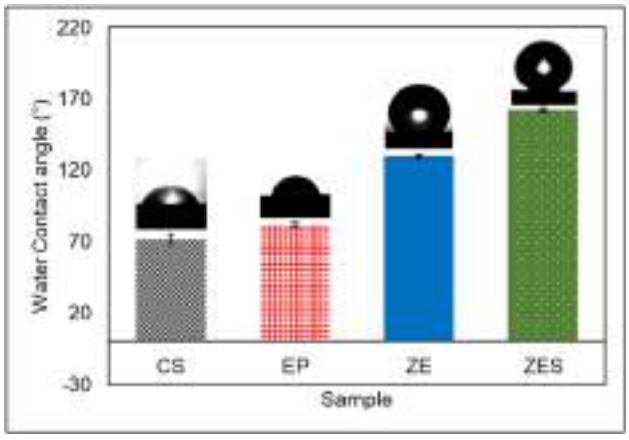

Fig. 9 – WCA results of the blank CS, and coated samples EP, ZE, and ZES.

3.3. *Electrochemical test*

3.3.1. *OCP measurements*

To study the corrosion behavior of the coating, the samples were immersed in 3.5 wt% NaCl aqueous solution. When a metal is exposed to the electrolyte, an electrochemical potential develops over time. The common factors that influence the OCP of a coated metal are defined by the anodic reactions, cathodic reactions, and electrolyte resistance [54]. OCP is often used to investigate the corrosion trend of a coating [40]. Higher OCP values often indicate a lower corrosion trend. The OCP results versus time for the uncoated and coated CS samples during the initial hour were presented in Fig. 10. As presumed, for the blank CS substrate, the OCP trend exhibited more negative values ranging at −0.66 ± 0.03 V (vs. SCE) than the coated samples, indicating higher susceptibility to corrosion. The decreasing trend shown in the first 1200s was ascribed to the continuous penetration of the corrosive medium and the dissolution process of the CS metal [16]. Subsequently, the OCP trend reaching a metastable state for the rest of the immersion time reveals that the sample was saturated and stabilized in the electrolyte. In the case of the coated samples, the higher OCP trends imply that the coated samples exhibited less susceptibility to the electrolyte. Furthermore, the OCP trends remained at relatively stable values during the whole period of 3600 s, demonstrating the effectiveness of the protection of these coatings in the electrolyte. Notably, compared to the regular samples with values of - 0.31 ± 0.013 V (vs. SCE) and - 0.26 ± 0.011 V (vs. SCE), for EP and ZE samples, respectively, the SHB ZES presented more noble OCP values of - 0.05 ± 0.002 V (vs. SCE) throughout the time interval, implying the least susceptibility of the SHB ZES coating to corrosion compared to the regular coating. This could relate to the highly protective nature of the SHB sample.

3.3.2. *EIS measurements*

EIS was employed for a more intuitive understanding of the barrier performance and corrosion behaviors of the coatings, which cannot be visualized, referring to the electrochemical reactions that happen within the metal and electrolyte interface [55]. Figs. 11 and 12 present the EIS plots of the blank CS substrate and the coating samples in 3.5% wt. NaCl solution.

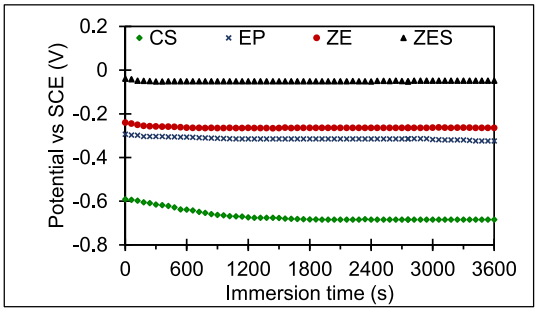

Fig. 10 – Open circuit potential (OCP vs SCE) results in immersion time in a 3.5% NaCl solution.

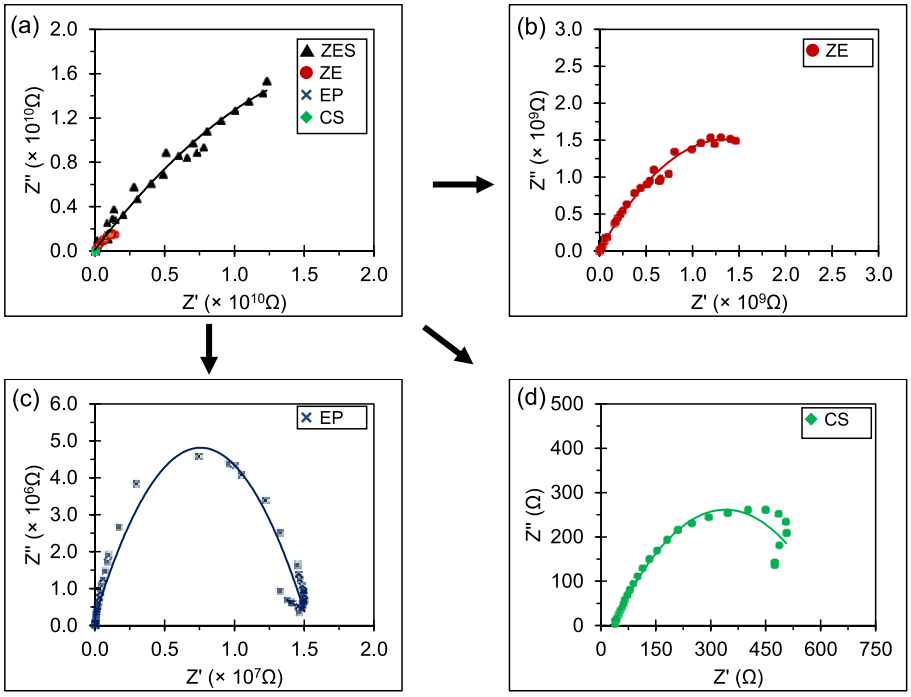

Fig. 11 – (a) the combined Nyquist plots of all samples; magnified diagram demonstrating respective Nyquist plots of the (b) ZE, (c) EP, and (d) blank CS substrate found in higher-frequency range.

Fig. 11a showed the combined Nyquist plots of the samples, whereas b-d showed the respective Nyquist of the ZE, EP, and CS substrate samples. Generally, the diameter of the capacitive arc is an indication of protection performance, which is directly proportional to the corrosion protection ability [56]. It is also known that a semicircle corresponds to a time constant. The blank CS substrate (Fig. 11a and d), showed the smallest capacitive loop compared to all other samples, revealing its poor corrosion resistance behavior. There is only one time constant in its Nyquist plot, suggesting that there is only one electrochemical process that happened on the metal surface. In the case of the coated samples, the semicircle diameters were much larger compared to that of the blank CS substrate, indicating the improved corrosion resistance of the coatings to the CS substrate. Notably, the semicircle diameter of the SHB ZES was the largest among all coated samples, indicating its excellent barrier performance. For the ZE sample (Fig. 11b), the smaller diameter of the capacitive arc due to the smaller ohmic resistance values implies the relatively weaker barrier performance of the coating compared to the ZES sample. Whereas for the EP sample as shown in Fig. 11c, the Nyquist plot presenting a full semicircle which typically consists of double-layer capacitance (C_{dl}) and charge transfer resistance (R_{ct}) elements indicates marked deterioration in the coating's barrier performance, which eventually leads to corrosion of the substrate. In addition, a closer examination also reveals the presence of a smaller arc at the higher frequencies. These two constants overlapped each other and were difficult to be identified due to the relatively small electrochemical reaction (charge transfer) across the metal/coating interface, and the first time constant corresponds to the impedance of coating is near to the second time constant caused by the Faraday process [57]. Besides that, the presence of the two-time constant also indicates the diffusion process of the electrolyte has begun [58]. The poor barrier performance can be explained following the examination of the coating structure discussed previously. Although plain EP is capable to provide a physical barrier to delay the permeation of

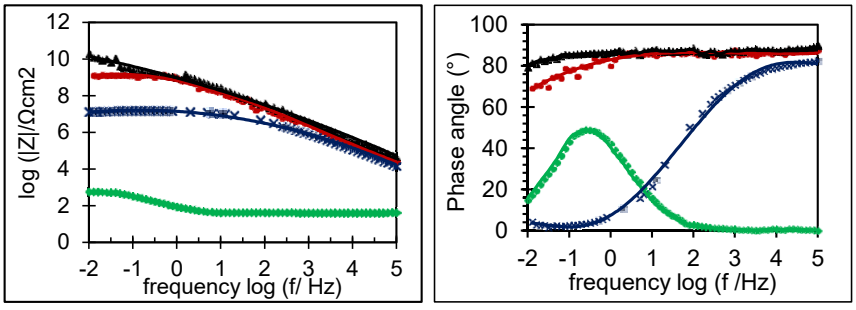

Fig. 12 – (a) Bode modulus plots, and (b) Bode of phase angle plots for all samples.

electrolytes, yet, barrier protection against corrosive ions is still inefficient on its own due to the presence of micropores.

The bode-modulus and bode-phase plots were presented in Fig. 12. It is known that in the bode-modulus plot, the impedance modulus value (|Z|) at the lowest frequency ($|Z|_{0.01Hz}$) can be a useful semi-quantitative indicator to evaluate the barrier performance of a coating and a bigger $|Z|_{0.01Hz}$ value points to a better corrosion resistance performance [39]. Overall, the SHB ZES sample exhibited the highest $|Z|_{0.01Hz}$ value approaching ~10^{10} Ωcm^2, which is by 8 orders of magnitude higher than blank CS substrate (~10^2 Ωcm^2), and 1-3 orders of magnitude higher than that of the regular coating samples (~10^9 Ωcm^2 and ~10^7 Ωcm^2 for ZE and EP, respectively), indicating its far superior improvement in corrosion protection for the CS substrate with the introduction of superhydrophobicity to the coating. On the other hand, the regular coating samples (ZE and EP) exhibited marginal plateaus in the low frequencies, indicating that the coatings were affected by the continuous permeation of the corrosive medium. In the case of the EP sample, the lower plateau shown in the mid frequencies suggests the appearance of the resistive region which may relate to the charge transfer process across the coating/metal interface. This indicates the deterioration of barrier performance has created a pathway that allows the permeation of electrolytes to reach the underlying metal.

In the bode-phase plot, each peak that appeared correlates to a time constant [18]. The high-frequency constant is assigned to the response from the coating, while the low-frequency constant corresponds to the corrosion process [39]. As shown in Fig. 11b, the peak appearing at about 10Hz in the phase angle plot of the blank CS sample is ascribed to the double-layer capacitance on the coating/substrate interface. This also implies the corrosion activity of the CS conditioned in the 3.5 wt % NaCl solution. For the EP sample, the phase plot exhibited features with two-time constants corresponding to both capacitances of coatings and the corrosion response of CS, implying the loss of the coating's barrier function. This could be due to the intrinsic nature of EP polymer which contains a lot of micropores and defects in itself that leads to loss of coating adhesion, allowing the diffusion of electrolyte into the coating [59]. As for the ZE sample, only a one-time constant appeared in its plot indicating better barrier performance of the composite coating than the plain EP. The barrier performance is attributed to the randomly dispersed ZnO nanoparticles that have filled the matrix and created a tortuous diffusion pathway for the corrosive ions to reach the

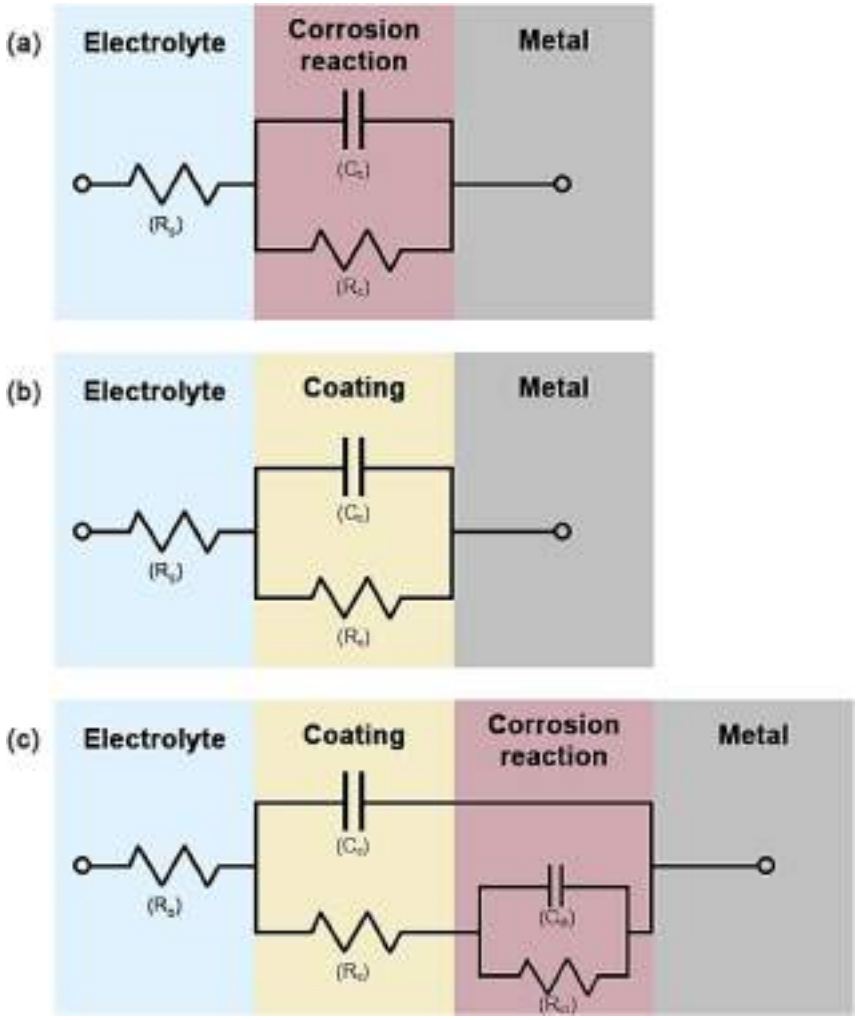

Fig. 13 – Electrical equivalent circuit for fitting EIS spectra of the (a) bare CS substrate, (b) ZES, and (c) for EP and ZE samples.

Table 1 – Electrochemical parameters fitted from the equivalent circuit.

Sample	R_c (Ω cm^2)	Q_c (S/cm^2 s^n)	n	R_{ct} (Ωcm^2)	Q_{dl} (S/cm^2 s^n)	n
CS	–	–	–	5.97×10^2	0.35×10^{-2}	0.82
EP	0.96×10^7	7.18×10^{-7}	0.80	1.57×10^7	1.43×10^{-6}	0.72
ZE	1.28×10^9	7.93×10^{-10}	0.95	2.37×10^9	2.93×10^{-9}	0.44
ZES	5.83×10^{10}	2.73×10^{-11}	0.77	–	–	–

underlying metal. However, a decline in the low frequencies can be found indicating minor deterioration is detected in the coating's barrier performance. Anyhow, the defect is negligible. On the other hand, for the ZES sample, only minimal decline in the phase angle value were observed in the low frequencies demonstrates the excellent barrier performance of the SHB coating, therefore the corrosive medium was difficult to infiltrate the coating.

For further investigation, the EIS data were fitted by different equivalent circuit models as depicted in Fig. 13a-c. In these models, R_s stands for the solution resistance and is considered a less important parameter as it does not contain any relevant information about the coating system [60], while R_c is known as the coating resistance, measuring the ability of a coating to resist current flow and it reflects the barrier properties of the coating. R_{ct} is the resistance of charge transfer within the metal and electrolyte, corresponding to the corrosion taking place below the coating [61]. Furthermore, Q_c is the constant phase element representing the capacitance of coating and it reflects the water uptake of a coating, while Q_{dl} is the double-layer capacitance which is often used to describe the severity of coating degradation and correlates to the distribution of ionic charges at the interface [39]. The constant phase element Q is used to represent the capacitance making it more accurate to fit the given non-ideal behavior of coatings [62]. Q can be expressed as $Q = \omega^{-n}/Y_0$ (cos $n\,\pi/2 + j$ sin $n\,\pi/2$) [63]. The parameter ω is the angular frequency, and Y_0 and n are the modulus and phase, respectively. The simple model R_s (Q_{dl} R_{ct}) as shown in Fig. 13a is used to fit the corrosion process of the blank CS due to its one-time constant in its EIS plots. The model R_s (Q_c R_c) as depicted in Fig. 13b is used to fit the spectra of the ZES sample in which no corrosion process can be detected due to the exceptional barrier performance. While in the case when there emerged two-time constants in the EIS plots, pointing out that the electrolyte has begun to infiltrate the coating and reach the underlying metal, the model R_s (C_c R_c (C_{dl} R_{ct}) as shown in Fig. 12c is used. This model fits the spectra of the regular coatings (EP and ZE). The electrical parameters interpreted from the fitting results are listed in Table 1.

R_{ct} and Q_{dl} are essential criteria that reflect the corrosion activities of the samples. The R_{ct} of the blank CS substrate exhibits only 597 Ω cm^2. The regular coating samples exhibit higher R_{ct} values, 1.57×10^7 Ω cm^2 and 7.04×10^{10} Ω cm^2 for EP and ZE samples, respectively, indicating higher corrosion protection for the CS substrate. In addition, the reduction in Q_{dl} values of the regular coatings to 0.40×10^{-6} S/cm^2 s^n (EP) and 1.10×10^{-9} S/cm^2 s^n (ZE) that are formerly from 0.0040 F/cm^2 in the CS metal, confirms that the regular coatings exhibited lower electrolyte uptake, indicating the charge transfer is more difficult to happen. Meanwhile, for the ZES sample, both R_{ct} and Q_{dl} are absent, implying that no corrosion process can be detected owing to the exceptional barrier properties as a result of the entrapped air in the coating. On the other hand, both R_c and Q_c can be studied for a more in-depth comparison of the protection performance of the coatings. These parameters are often related to the coating defects and pores that could be the channel for the diffusion of electrolytes reaching the coating/substrate interface [39]. Among the coating samples, ZES exhibited the highest R_c value 5.83×10^{10} Ω cm^2, which increased by an order for the ZE sample (1.28×10^9 Ω cm^2) and 3 orders of magnitude for the EP sample (0.96×10^7 Ω cm^2), implying the evidence of the distinctive barrier portrayed by the SHB surface. Reversely, the ZES sample exhibited the least Q_c value indicating the least electrolyte penetration of the SHB ZES. In contrast, the Q_c value showed the highest in the EP sample (7.18×10^{-7} S/cm^2 s^n), reflecting the most water uptake in its coating .This reveals the higher porosity in the EP coating which was in line with the morphological results of the EP sample discussed previously. Anyhow, it is interesting to note that the as-prepared SHB ZES coating offers an exceptionally high R_c of ~10^{10} Ω cm^2, which is comparable to or even outperformed most of any other SHB EP-based composite coatings on the metals reported in this recent [56,64–66].

3.3.3. *Tafel measurements*

The potentiodynamic polarization (PDP) curve also known as the Tafel plot is useful for rapid appraisal of the instantaneous corrosion rate of the electrolyte concerning the metal. The Tafel plots of the blank CS, EP, ZE, and ZES coated samples are shown in Fig. 14. The main parameters in the Tafel data, involving the corrosion potential (E_{corr}), corrosion current density (I_{corr}), polarization resistance (R_p), and corrosion rate (R_{corr}), derived by the extrapolation method are presented in Table 2. In a typical Tafel curve, a more positive E_{corr}

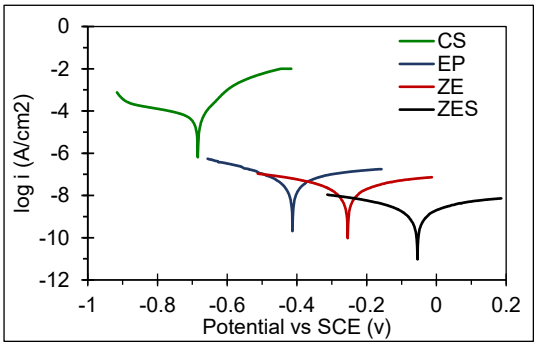

Fig. 14 – Potentiodynamic polarization curves of blank CS substrate, plain EP, ZE, and ZES coated samples.

Table 2 – Analysis results of Tafel polarization curves of the samples immersed in 3.5 wt % NaCl solution.

Sample	E_{corr} (V vs. SCE)	β_a (V/dev)	β_b (V/dev)	I_{corr} (A/cm^2)	R_p (Ω/cm^2)	R_{corr} (mm/year)
CS	−0.68	0.048	0.151	1.09E-04	365.40	1.27
EP	−0.41	0.034	0.109	3.82E-08	9.30E+05	0.44E-03
ZE	−0.25	0.009	0.016	3.15E-10	6.16E+06	9.08E-06
ZES	−0.05	0.004	0.006	2.08E-11	7.71E+07	3.38E-07

corresponds to a lower corrosion tendency, while a smaller I_{corr} corresponds to a lower corrosion rate [67]. In addition, the R_p is considered the overall effect of I_{corr}, and a high R_p implies high corrosion resistance. The R_p (Ω/cm^2) is calculated based on the Stern-Geary relationship as follows [68]:

$$R_p = \frac{\beta_a \times \beta_c}{2.3\ \text{Icorr}\ (\beta_a + \beta_c)} \quad (1)$$

where β_a and β_c denote the Tafel slopes in the anodic branch and cathodic branch respectively determined from the integrated software. Furthermore, the R_{corr} (mm/year) is calculated according to the following equation [69]:

$$R_{corr} = \frac{k\, MI_{corr}}{\rho_m} \quad (2)$$

where M_n and ρ_m represent equivalent weight (27.925 g/mol) and density (7.86 g/cm^3) of the substrate respectively, whereas, k denotes the constant (3268.6 mol/A).

According to the fitted results (Table 2), the E_{corr} and I_{corr} of the CS substrate were-0.68 and 1.09 × 10^{-4}, respectively. For all the coated samples, the E_{corr} shifted to more positive values, whereas the I_{corr} shifted to lower values, indicating less corrosion tendency and improved corrosion resistance, in comparison to the bare CS substrate. Notably, among the coated samples, the I_{corr} of the ZES sample showed the least value of 2.08 × 10^{-11} A cm^{-2}, as well as the most positive E_{corr} value of −0.05, verifying the better corrosion protection of the SHB ZES coating than the regular coating samples with lower hydrophobicity. Even though, the decrease in I_{corr} and the shifting to the more positive direction in E_{corr} of the regular coated samples also show an improvement in corrosion resistance to the CS substrate. Yet, their performance is limited compared to the SHB coating. This may be related to the weaker hydrophobicity, thus having a higher tendency for permeation of electrolytes. Nevertheless, the R_{corr} of the regular coatings still exhibited a reduction in values (0.44 × 10^{-3} and 9.08 × 10^{-6} for EP and ZES) by 3 and 6 orders of magnitude, respectively, demonstrating their competency in corrosion protection. Howbeit, the R_{corr} of the ZES which was 3.38 × 10^{-7} mm/year, has shown a reduction by 7 orders of magnitude compared to the blank CS substrate (1.27 mm/year). This further verified the far superior corrosion protection offered by the SHB ZES to the CS substrate.

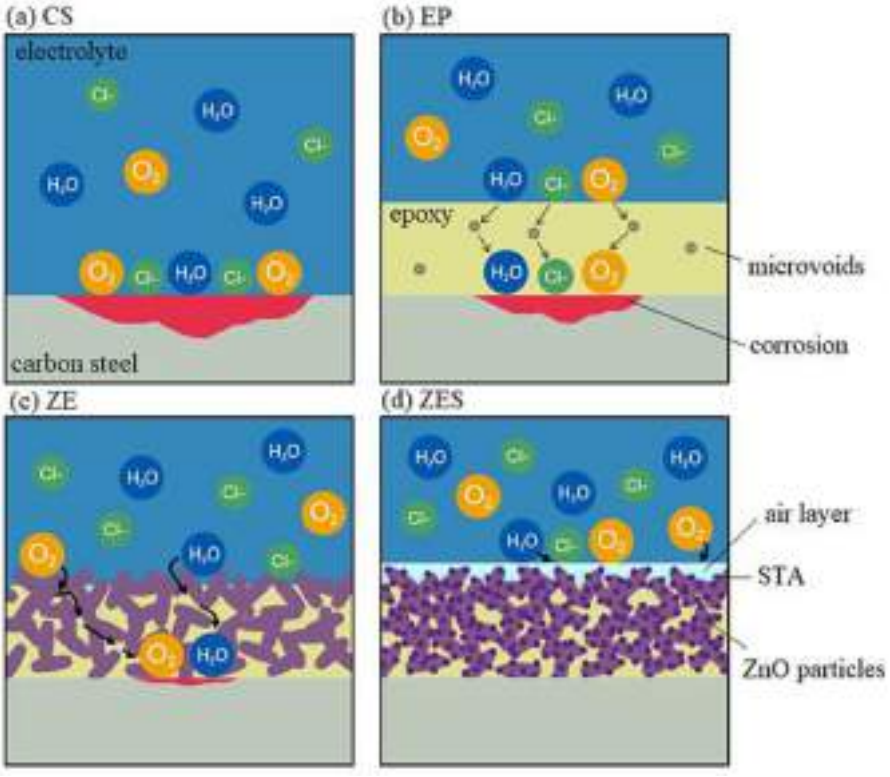

Fig. 15 – Schematic diagrams of the corrosion mechanism of (a) blank CS, (b) EP, (c) ZE, and, (d) ZES-coated samples.

3.3.4. *Corrosion mechanism*

It is known that the corrosion of metal is a degradation process resulting from the electrochemical reaction with the surrounding medium. When the blank CS substrate is exposed to the corrosive medium, namely 3.5% wt. NaCl solution, the electrolyte can freely reach the entire surface, and the corrosive factors such as H_2O, Cl^-, O_2, and H_2 are available to react with the surface, therefore damaging the metal, as illustrated in Fig. 15a. For the plain EP sample, the corrosive media can be delayed momentarily, however, the barrier is still deficient as the ions are prone to permeate the micro-holes of the coating due to the intrinsic nature of EP, therefore initiating the redox reaction and thus failed the coating (Fig. 15b) [70]. In the case of the ZE sample, the corrosion barrier was slightly improved owing to the improvement in hydrophobic properties which could greatly insulate the contact between the corrosive media and the CS metal. The hydrophobicity of the coating is attributed to the intense aggregation of ZnO NP embedding in the EP matrix which promotes the surface roughness of the coating. Besides that, these heterogeneously dispersed ZnO nanoparticles improved the compactness of the coating, creating a more circuitous pathway for the corrosive factor to infiltrate the coating to reach the underlying substrate, therefore, demonstrating adequate corrosion resistance to the metal. After all, the EIS and PDP results of the ZES have proven notable improvements in the resistance of coating against corrosion with the introduction of SHB properties. In this case, the presence of the air film, which has been confirmed by the 3D LSCM and mirror test discussed previously plays the most crucial role in imparting barrier performance to the coating. When immersed in the electrolyte, the air interlayer captured within the coating/electrolyte interface promotes Cassie contact and forms an additional non-conductive barrier to the as-prepared SHB ZES, which to an extent isolates the surface from the electrolyte, therefore explaining the results of OCP which is very closed to 0 and high $|Z|_{0.01Hz}$ result approaching 10^{10} Ωcm^2. Besides that, the superior inhibitive effect of the SHB ZES is also proven by the PDP results, in which the I_{corr} value is suppressed down to 2.08×10^{-11} A/cm^2, thereby achieving an excellent corrosion rate result of 3.38×10^{-7} mm/year.

4. Conclusion

Superhydrophobic (SHB) coating composed of ZnO nanoparticles, epoxy (EP), and stearic acid (STA) was fabricated on the S50C carbon steel substrate with a direct yet effective one-step coating deposition method. The aggregation of ZnO nanoparticles in EP promotes the construction of hierarchical micro/nanoscale rough structures on the surface and the incorporation of STA into the matrix transforms the surface to SHB thus improving its anticorrosion performance. Results of WCA showed a high value of $165.13 \pm 1.5^\circ$ indicating superior superhydrophobicity of the coating. According to the corrosion results, the I_{corr} of the SHB sample (ZES) with value exhibits a decrement from 1.09×10^{-4} A/cm^2 of uncoated CS to 2.08×10^{-11} A/cm^2. The corrosion rate of the SHB sample achieved an excellent result of 6.4971×10^{-6} mm per year as compared to the blank CS substrate of 0.07699 mm per year. In addition, the ZES sample significantly improved its anticorrosive performance in terms of higher impedance modulus and larger capacitive arc, both at least by 1 order of magnitude, as compared with those regular plain EP and regular coating, which is attributed to the excellent barrier effect from the SHB surface. Overall results show the SHB surface is stable against exposure to a corrosive medium due to the existence of an intact and retained barrier layer composed of entrapped air on the surface. This superhydrophobic coating shows exceptional corrosion resistance is of high application potential in the marine environment for mitigating corrosion in seawater in the short term. Future research should prioritize conducting prolonged corrosion tests to gain a comprehensive understanding of the coating's durability under realistic environmental conditions.

Declaration of competing interest

The authors declare that they have no known competing financial interests or personal relationships that could have appeared to influence the work reported in this paper.

Acknowledgment

The authors gratefully acknowledge the financial support from the Ministry of Higher Education Malaysia under the FRGS Grant with Project Number FRGS/1/2021/TK0/UMP/02/48 and Universitas Muhammadiyah Ponorogo under the Fundamental Research Grant with Project Number #066/VI.4/PN/2023.

REFERENCES

[1] Pandiyarajan S, Ganesan M, Liao A-H, Manickaraj SSM, Huang S-T, Chuang H-C. Ultrasonic-assisted supercritical-CO2 electrodeposition of Zn-Co film for high-performance corrosion inhibition: a greener approach. Ultrason Sonochem 2021:72 105463.

[2] Masmiati N, Sarhan AA, Hassan MAN, Hamdi M. Optimization of cutting conditions for minimum residual stress, cutting force and surface roughness in end milling of S50C medium carbon steel. Measurement 2016;86:253–65.

[3] Lgaz H, Chung I-M, Albayati MR, Chaouiki A, Salghi R, Mohamed SK. Improved corrosion resistance of mild steel in acidic solution by hydrazone derivatives: an experimental and computational study. Arab J Chem 2020;13(1):2934–54.

[4] Chen S, Li B, Xiao R, Luo H, Yu S, He J, Liao X. Design an epoxy coating with TiO2/GO/PANI nanocomposites for enhancing corrosion resistance of Q235 carbon steel. Materials 2021;14(10):2629.

[5] Liu X, Jie H, Liu R, Liu Y, Li T, Lyu K. Research on the preparation and anticorrosion properties of EP/CeO2-GO nanocomposite coating. Polymers 2021;13(2):183.

[6] Zhang W, Liao D, Tang D, Han E, Wang J. Study on corrosion behavior of Ni–P/Ni–Cu–P superhydrophobic composite coatings preparation on L360 steel by two-step method. J Mater Res Technol 2023;23:3035–47.

[7] Wahby MH, Atta AM, Moustafa YM, Ezzat AO, Hashem AI. Hydrophobic and superhydrophobic bio-based nano-magnetic epoxy composites as organic coating of steel. Coatings 2020;10(12):1201.
[8] Zhang Z, Zhao N, Qi F, Zhang B, Liao B, Ouyang X. Reinforced superhydrophobic anti-corrosion epoxy resin coating by fluorine–silicon–carbide composites. Coatings 2020;10(12):1244.
[9] Xu Y, Gao D, Dong Q, Li M, Liu A, Wang X, Wang S, Liu Q. Anticorrosive behavior of epoxy coating modified with hydrophobic nano-silica on phosphatized carbon steel. Prog Org Coating 2021:151 106051.
[10] Ma Q, Wang W, Dong G. Facile fabrication of biomimetic liquid-infused slippery surface on carbon steel and its self-cleaning, anti-corrosion, anti-frosting and tribological properties. Colloids Surf A Physicochem Eng Asp 2019;577:17–26.
[11] Ma Q, Tong Z, Wang W, Dong G. Fabricating robust and repairable superhydrophobic surface on carbon steel by nanosecond laser texturing for corrosion protection. Appl Surf Sci 2018;455:748–57.
[12] Wang H, He M, Liu H, Guan Y. One-step fabrication of robust superhydrophobic steel surfaces with mechanical durability, thermal stability, and anti-icing function. ACS Appl Mater Interfaces 2019;11(28):25586–94.
[13] Cho E-C, Chang-Jian C-W, Chen H-C, Chuang K-S, Zheng J-H, Hsiao Y-S, Lee K-C, Huang J-H. Robust multifunctional superhydrophobic coatings with enhanced water/oil separation, self-cleaning, anti-corrosion, and anti-biological adhesion. Chem Eng J 2017;314:347–57.
[14] Amiriafshar M, Rafieazad M, Duan X, Nasiri A. Fabrication and coating adhesion study of superhydrophobic stainless steel surfaces: the effect of substrate surface roughness. Surfaces and Interfaces; 2020. p. 20 100526.
[15] Zhou H, Chen R, Liu Q, Liu J, Yu J, Wang C, Zhang M, Liu P, Wang J. Fabrication of ZnO/epoxy resin superhydrophobic coating on AZ31 magnesium alloy. Chem Eng J 2019;368:261–72.
[16] Zhang D, Qian H, Wang L, Li X. Comparison of barrier properties for a superhydrophobic epoxy coating under different simulated corrosion environments, vol. 103. Corrosion science; 2016. p. 230–41.
[17] Han X, Peng J, Jiang S, Xiong J, Song Y, Gong X. Robust superamphiphobic coatings based on raspberry-like hollow SnO2 composites. Langmuir 2020;36(37):11044–53.
[18] Yang Z, Wang L, Sun W, Li S, Zhu T, Liu W, Liu G. Superhydrophobic epoxy coating modified by fluorographene used for anti-corrosion and self-cleaning. Appl Surf Sci 2017:401 146–155.
[19] Cao K, Yu Z, Zhu L, Yin D, Chen L, Jiang Y, Wang J. Fabrication of superhydrophobic layered double hydroxide composites to enhance the corrosion-resistant performances of epoxy coatings on Mg alloy. Surf Coating Technol 2021:407 126763.
[20] Xu S, Wang Q, Wang N. Eco-friendly fabrication of superhydrophobic surface with anti-corrosion by transferring dendrite-like structures to aluminum substrate. Colloids Surf A Physicochem Eng Asp 2020:124719.
[21] Guo C, Ding H, Xie M, Zhang H, Hong X, Sun L, Ding F. Multifunctional superamphiphobic fluorinated silica with a core-shell structure for anti-fouling and anti-corrosion applications. Colloids Surf A Physicochem Eng Asp 2021:615 126155.
[22] Xiong D, Liu G, Duncan ES. Robust amphiphobic coatings from bi-functional silica particles on flat substrates. Polymer 2013;54(12):3008–16.
[23] Su C. A simple and cost-effective method for fabricating lotus-effect composite coatings. J Coating Technol Res 2012;9(2):135–41.
[24] Guo X, Guo R, Fang M, Wang N, Liu W, Pei H, Liu N, Mo Z. A novel composite protective coating with UV and corrosion resistance: load floating and self-cleaning performance. Ceram Int 2022;48(12):17308–18.
[25] Wang J, Pei X, Zhang J, Liu S, Li Y, Wang C. Reversible switch of wettability of ZnO@ stearic acid nanoarray through alternative irradiation and heat-treatment. Ceram Int 2021;47(7):9164–8.
[26] Gurav AB, Latthe SS, Vhatkar RS, Lee J-G, Kim D-Y, Park J-J, Yoon SS. Superhydrophobic surface decorated with vertical ZnO nanorods modified by stearic acid. Ceram Int 2014;40(5):7151–60.
[27] Czyżowska A, Barbasz A. A review: zinc oxide nanoparticles–friends or enemies? Int J Environ Health Res 2022;32(4):885–901.
[28] Faizan M, Hayat S, Pichtel J. Effects of zinc oxide nanoparticles on crop plants: a perspective analysis. Sustainable Agriculture Reviews 2020;41:83–99. Springer.
[29] Zhang X, Si Y, Mo J, Guo Z. Robust micro-nanoscale flowerlike ZnO/epoxy resin superhydrophobic coating with rapid healing ability. Chem Eng J 2017;313:1152–9.
[30] Darband GB, Aliofkhazraei M, Khorsand S, Sokhanvar S, Kaboli A. Science and engineering of superhydrophobic surfaces: review of corrosion resistance, chemical and mechanical stability. Arab J Chem 2020;13(1):1763–802.
[31] Li M, Liu N, Chen J, Li Q. Simple construction based on epoxy-bonded super-hydrophobic anti-corrosion coating. J Taiwan Inst Chem Eng 2019;95:682–91.
[32] Wang H, Di D, Zhao Y, Yuan R, Zhu Y. A multifunctional polymer composite coating assisted with pore-forming agent: preparation, superhydrophobicity and corrosion resistance. Prog Org Coating 2019;132:370–8.
[33] Wu Y, Jia S, Wang S, Qing Y, Yan N, Wang Q, Meng T. A facile and novel emulsion for efficient and convenient fabrication of durable superhydrophobic materials. Chem Eng J 2017;328:186–96.
[34] Nguyen DM, Vu TN, Nguyen TML, Nguyen TD, Thuc CNH, Bui QB, Colin J, Perré P. Synergistic influences of stearic acid coating and recycled PET microfibers on the enhanced properties of composite materials. Materials 2020;13(6):1461.
[35] Rahmani M, Ghasemi FA, Payganeh G. Effect of surface modification of calcium carbonate nanoparticles on their dispersion in the polypropylene matrix using stearic acid. Mechanics & Industry 2014;15(1):63–7.
[36] Li Y, Weng W. Surface modification of hydroxyapatite by stearic acid: characterization and in vitro behaviors. J Mater Sci Mater Med 2008;19(1):19–25.
[37] Yap SW, Johari N, Mazlan SA, Hassan NA. Mechanochemical durability and self-cleaning performance of zinc oxide-epoxy superhydrophobic coating prepared via a facile one-step approach. Ceram Int 2021;47(11):15825–33.
[38] Standard A. G61-86, Standard test method for conducting cyclic potentiodynamic polarization measurements for localized corrosion susceptibility of iron-, nickel-, or cobalt-based alloys. Philadelphia, PA, USA: ASTM standards, ASTM; 2009.
[39] Zhao H, Ding J, Liu P, Yu H. Boron nitride-epoxy inverse "nacre-like" nanocomposite coatings with superior anticorrosion performance. Corrosion Science; 2021. p. 183 109333.
[40] Ye Y, Zhang D, Liu T, Liu Z, Liu W, Pu J, Chen H, Zhao H, Li X. Improvement of anticorrosion ability of epoxy matrix in simulate marine environment by filled with

superhydrophobic POSS-GO nanosheets. J Hazard Mater 2019;364:244–55.
[41] Seeharaj P, Sripako K, Promta P, Detsri E, Vittayakorn N. Facile and eco-friendly fabrication of hierarchical superhydrophobic coating from eggshell biowaste. Int J Appl Ceram Technol 2019;16(5):1895–903.
[42] Zhang J, Wang J, Zhang B, Zeng Y, Duan J, Hou B. Fabrication of anodized superhydrophobic 5083 aluminum alloy surface for marine anti-corrosion and anti-biofouling. Journal of Oceanology and Limnology 2020;38(4):1246–55.
[43] Lou C, Zhang R, Lu X, Zhou C, Xin Z. Facile fabrication of epoxy/polybenzoxazine based superhydrophobic coating with enhanced corrosion resistance and high thermal stability. Colloids Surf A Physicochem Eng Asp 2019:562 8–15.
[44] Zhou Y, Ma Y, Sun Y, Xiong Z, Qi C, Zhang Y, Liu Y. Robust superhydrophobic surface based on multiple hybrid coatings for application in corrosion protection. ACS Appl Mater Interfaces 2019;11(6):6512–26.
[45] Prontera CT, Sico G, Montanino M, De Girolamo Del Mauro A, Tassini P, Maglione MG, Minarini C, Manini P. Sustainable, fluorine-free, low cost and easily processable materials for hydrophobic coatings on flexible plastic substrates. Materials 2019;12(14):2234.
[46] Tuong VM, Huyen NV, Kien NT, Dien NV. Durable epoxy@ ZnO coating for improvement of hydrophobicity and color stability of wood. Polymers 2019;11(9):1388.
[47] de Lucas-Gil E, Menendez J, Pascual L, Fernandez JF, Rubio-Marcos F. The benefits of the ZnO/clay composite formation as a promising antifungal coating for paint applications. Appl Sci 2020;10(4):1322.
[48] Wu Y, Wu X, Yang F, Ye J. Preparation and characterization of waterborne UV lacquer product modified by zinc oxide with flower shape. Polymers 2020;12(3):668.
[49] Dou Q, Wong KW, Li Y, Ng KM. Novel nanosheets of ferrite nanoparticle arrays in carbon matrix from single source precursors: an anode material for lithium-ion batteries. J Mater Sci 2018;53(6):4456–66.
[50] Seth M, Khan H, Bhowmik R, Karmakar S, Jana S. Facile fabrication of fluorine free zirconium zinc stearate based superhydrophobic and superoleophilic coating on cotton fabric with superior antibacterial property. J Sol Gel Sci Technol 2020;94(1):127–40.
[51] Zhu W, Wu Y, Zhang Y. Fabrication and characterization of superhydrophobicity ZnO nanoparticles with two morphologies by using stearic acid. Mater Res Express 2019;6(11):1150d1151.
[52] Zheng S, Bellido-Aguilar DA, Huang Y, Zeng X, Zhang Q, Chen Z. Mechanically robust hydrophobic bio-based epoxy coatings for anti-corrosion application. Surf Coating Technol 2019;363:43–50.
[53] Wei H, Xia J, Zhou W, Zhou L, Hussain G, Li Q, Ostrikov KK. Adhesion and cohesion of epoxy-based industrial composite coatings. Compos B Eng 2020;193:108035.
[54] Manoj A, Ramachandran R, Menezes PL. Influence of abrasive load on wettability and corrosion inhibition of a commercial superhydrophobic coating. Coatings 2020;10(9):887.
[55] Wang L, Zong Q, Sun W, Yang Z, Liu G. Chemical modification of hydrotalcite coating for enhanced corrosion resistance, vol. 93. Corrosion Science; 2015. p. 256–66.
[56] Ren T, Tang G, Yuan B, Yan Z, Ma L, Huang X. One-step fabrication of robust superhydrophobic coatings with corrosion resistance by a self-curing epoxy-resin-based adhesive. Surface and Coatings Technology; 2019. p. 380 125086.
[57] Zhang B, Li J, Zhao X, Hu X, Yang L, Wang N, Li Y, Hou B. Biomimetic one step fabrication of manganese stearate superhydrophobic surface as an efficient barrier against marine corrosion and Chlorella vulgaris-induced biofouling. Chem Eng J 2016;306:441–51.
[58] Ghazali N, Basirun WJ, Mohammed Nor A, Johan MR. Super-amphiphobic coating system incorporating functionalized nano-Al2O3 in polyvinylidene fluoride (PVDF) with enhanced corrosion resistance. Coatings 2020;10(4):387.
[59] Serenario MED, Santos BAF, Miranda LRMd, Bueno AHS. Evaluation of the anticorrosive behavior of epoxy-Nb2O5 paint in high temperatures submitted to the environment with sulfuric acid. J Coating Technol Res 2020;17(5):1331–42.
[60] Cui M, Ren S, Chen J, Liu S, Zhang G, Zhao H, Wang L, Xue Q. Anticorrosive performance of waterborne epoxy coatings containing water-dispersible hexagonal boron nitride (h-BN) nanosheets. Appl Surf Sci 2017;397:77–86.
[61] Situ Y, Guo Y, Ji W, Liu D, Wei D, Huang H. Polyaniline encapsulated α-zirconium phosphate nanosheet for enforcing anticorrosion performance of epoxy coating. J Coating Technol Res 2021;18(4):999–1012.
[62] Van Westing E, Ferrari G, De Wit J. The determination of coating performance with impedance measurements—II. Water uptake of coatings. Corrosion Sci 1994;36(6): 957–77.
[63] Nishikata A, Ichihara Y, Hayashi Y, Tsuru T. Influence of electrolyte layer thickness and pH on the initial stage of the atmospheric corrosion of iron. J Electrochem Soc 1997;144(4):1244.
[64] Yuan S, Zhao X, Jin Z, Liu N, Zhang B, Wang L, Duan J, Hou B. Fabrication of an environment-friendly epoxy coating with flexible superhydrophobicity and anti-corrosion performance. Colloids Surf A Physicochem Eng Asp 2022:633 127545.
[65] Wei R, Liu Z, Wei W, Wang S, Lv Y-j, Han G-C. Anticorrosion performance of hydrophobic acid-modified-MOFs/epoxy coatings. Colloid and Interface Science Communications 2022;46:100580.
[66] Li D-W, Wang H-Y, Liu Y, Wei D-S, Zhao Z-X. Large-scale fabrication of durable and robust super-hydrophobic spray coatings with excellent repairable and anti-corrosion performance. Chem Eng J 2019;367:169–79.
[67] Tong W, Karthik N, Li J, Wang N, Xiong D. Superhydrophobic surface with stepwise multilayered micro-and nanostructure and an investigation of its corrosion resistance. Langmuir 2019;35(47):15078–85.
[68] Xiong J, Sarkar DK, Chen X-G. Superhydrophobic honeycomb-like cobalt stearate thin films on aluminum with excellent anti-corrosion properties. Appl Surf Sci 2017;407:361–70.
[69] Chang C-H, Hsu M-H, Weng C-J, Hung W-I, Chuang T-L, Chang K-C, Peng C-W, Yen Y-C, Yeh J-M. 3D-bioprinting approach to fabricate superhydrophobic epoxy/organophilic clay as an advanced anticorrosive coating with the synergistic effect of superhydrophobicity and gas barrier properties. J Mater Chem 2013;1(44):13869–77.
[70] Zhan Y, Zhang J, Wan X, Long Z, He S, He Y. Epoxy composites coating with Fe3O4 decorated graphene oxide: modified bio-inspired surface chemistry, synergistic effect and improved anti-corrosion performance. Appl Surf Sci 2018;436:756–67.